AGU PUBLICATIONS

Geophysical Research Letters

RESEARCH LETTER

10.1002/2013GL059004

Key Points:
- Eddy APE can be thought as the covariance of density and isopycnal displacement
- Argo profiles are combined to estimate pointwise statistics
- EAPE reveals the structure and the magnitude of the oceanic interior turbulence

Correspondence to:
G. Roullet,
roullet@univ-brest.fr

Citation:
Roullet, G., X. Capet, and G. Maze (2014), Global interior Eddy Available Potential Energy diagnosed from Argo floats, *Geophys. Res. Lett.*, *41*, doi:10.1002/2013GL059004.

Received 11 DEC 2013
Accepted 24 JAN 2014
Accepted article online 30 JAN 2014

Global interior eddy available potential energy diagnosed from Argo floats

Guillaume Roullet[1], Xavier Capet[2], and Guillaume Maze[3]

[1]Laboratoire de Physique des Oceans, Université de Bretagne Occidentale, UMR6523, Brest, France, [2]IPSL/LOCEAN, CNRS/UPMC/IRD/MNHN, UM7159, Paris, France, [3]Laboratoire de Physique des Oceans, IFREMER, UMR6523, Plouzané, France

Abstract By combining all Argo profiles for the period 2002 to present, a cumulative density function is constructed on a 3-D grid of the global ocean. This function quantifies the statistics of isopycnals: time-averaged density, root-mean square of isopycnal displacement, and eddy available potential energy (EAPE). EAPE is the analogue of the eddy kinetic energy, but for the potential energy reservoir. Because it is essentially tied to the spatial structure and magnitude of mesoscale activity, EAPE is an important quantity that should be useful to evaluate eddy resolving/permitting model turbulence and circulation. Among other striking features are the turbulent behavior of Pacific and southern Atlantic Tsuchiya jets and subsurface EAPE maxima in some parts of the ocean, particularly in the Southern Ocean.

1. Introduction

In the mesoscale range (from 20 to 400 km), the ocean is highly turbulent. This turbulence is dominated by eddies that are continuously generated, interacting, merging, propagating, and ultimately dissipated. The chaotic behavior calls for a statistical approach. Detailed descriptions of the spatial structure of that turbulence rest primarily on eddy kinetic energy (EKE) obtained from satellite altimetry [*Ducet et al.*, 2000; *Chelton et al.*, 2007] through geostrophy. In particular, surface EKE is the central quantity to evaluate the realism of mesoscale turbulence in eddy-resolving models. No such energetic signal, genuinely observational, is available for the whole ocean interior.

We present here a measure of interior turbulence that is energetically meaningful and thus comparable to surface EKE. This measure is obtained by combining all Argo data available which restricts our study to the upper 2000 m. Previous similar studies, also using Argo data, described the variance of temperature and salinity [*Forget and Wunsch*, 2007; *Von Schuckmann et al.*, 2009] which are important measures of ocean interior variability but not purely dynamical quantities. *Forget and Wunsch* [2007] went beyond: They estimated the variance of isopycnal displacements and showed that the variance of sea level height was largely explained by interior variability. This study extends these results, focusing on the energy and taking advantage of the database growth.

The key point is that the mesoscale turbulence intensity can be estimated through its signature in terms of isopycnal displacement. To measure the energy stored in these vertical displacements we use the eddy available potential energy (EAPE) [*Lorenz*, 1955]. EAPE is generally estimated only on global average as one of the four boxes entering the Lorenz energy cycle [*von Storch et al.*, 2012]. In this paper we estimate a three-dimensional EAPE density based on the available potential energy density (APE) and a local reference profile. We consider the time mean density as reference state. This natural choice has the advantage of isolating the local temporal fluctuations of isopycnals from their large-scale sloping. It has, to our knowledge, never been used in this context. EAPE is thus the fraction of APE that would vanish if the isopycnals were steady. Its most important property is to be the analogue of EKE for potential energy.

Like EKE, it is in essence a covariance. The APE density definition depends on the set of equations used to describe the fluid dynamics [*Holliday and McIntyre*, 1980; *Shepherd*, 1993; *Tailleux*, 2012]. We have chosen the following practical definition:

$$\mathcal{V} = -\frac{g}{2\rho_0}\overline{\zeta'\,\rho'}\,, \tag{1}$$

where ζ' is the vertical isopycnal displacement, ρ' the density anomaly associated with this displacement, and the bar refers to long-term time averaging. Equation (1) is obtained by applying the trapezoidal rule on the primitive equations APE [*Holliday and McIntyre*, 1980]. Primes refer to the fluctuations from a time mean.

For small ζ' (1) coincides with the quasi-geostrophic definition of APE; for larger ζ' it is a better estimate of the APE density.

To estimate (1) we have adopted a statistical point of view. All available profiles are combined to determine the annual cumulative density function (CDF) $C(\rho; \mathbf{x}, z)$, measuring the probability that $\rho(\mathbf{x}, z, t) \leq \rho$ at horizontal location $\mathbf{x}$ and depth z. This function contains all the statistical information from which we can compute climatologies for EAPE and also $\bar{\rho}$, σ_ρ, σ_ζ (where σ stands for standard deviation). An important caveat is that the diagnostic does not distinguish the processes responsible for the density fluctuations. It is thus the result of mesoscale turbulence (eddies and Rossby waves), internal wave activity, and diabatic atmospheric forcing. These include variability generated through the seasonal cycles of wind and buoyancy forcing. The paper is organized as follows: the method is explained in section 2, results are presented in section 3, and a conclusion is given in section 4.

2. Method

The vertical isopycnal displacement ζ' should be estimated with the adiabatic compressibility effects removed. Among the several possible techniques at hand, we have chosen to use the virtual density [*Sun et al.*, 1999] $\rho_*(z) = \rho_{\text{is}}(z)/[1 + p(z)/(\rho_0 c^2)]$, where ρ_{is} is the in situ density computed with the 2010 EOS [*IOC et al.*, 2010], $\rho_0 = 1\,000\,\text{kg m}^{-3}$, $c = 1\,510\,\text{m s}^{-1}$ a reference sound speed, and $p(z)$ the function relating depth to pressure. It is a pressure-compensated EOS routinely used in ocean models such as the Hybrid Coordinate Ocean Model (HYCOM) [*Hallberg*, 2005] and Regional Ocean Modeling System (ROMS) [*Shchepetkin and McWilliams*, 2011].

The pointwise annual CDF is evaluated using

$$C(\mathbf{x}, z; \rho) = \frac{1}{n(\mathbf{x}, z)} \sum_{i \in \text{Argo}} W(|\mathbf{x} - \mathbf{x}^i|)\, H(\rho_*^i(z) < \rho)\,, \tag{2}$$

where $\rho_*^i(z)$ is the virtual density of Argo profile i, H is the step function, $W(d) = e^{-d^2/2\sigma^2}$ is a weight function, d the spherical distance between the Argo profile location $\mathbf{x}^i$ and the grid point $\mathbf{x}$, and $n(\mathbf{x}, z)$ is the normalization constant ensuring that $C(\mathbf{x}, z; \infty) = 1$. The spatial resolution of the grid is set through σ, the width of the weight function. In practice, the summation is truncated by keeping the profiles corresponding to $|\mathbf{x} - \mathbf{x}^i| < 6\sigma$. Because of the gaussian weight, each profile is used on average at 2π grid cells. The factor $n(\mathbf{x}, z)$ can be interpreted as the number of profiles used at location $(\mathbf{x}, z)$. It sets the significance of the statistical estimates: The better the spatial resolution (small σ) and the temporal resolution (e.g., monthly instead of annual), the lower the statistical significance.

About 830, 000 Argo profiles enter the calculation of the annual CDF. Results are not significantly affected by the value of σ between $1/2°$ and $2°$, apart from increased spatial details at the highest resolution. Because these details most often coincide with known hydrological features and not with places where n is small, we retain $\sigma = 0.5°$. We also discard the locations where statistical significance is questionable ($n < 10$). In very densely sampled regions, like in the Kurushio where $n \gtrsim 150$, it is even possible to estimate EAPE on a grid finer than $1/2°$.

From the CDF we define two probability density functions (PDFs): $P_E(\mathbf{x}, z; \rho) = \partial_\rho C(\mathbf{x}, z; \rho)$ the probability of having ρ at $(\mathbf{x}, z)$ and $P_L(\mathbf{x}, z; \rho) = \partial_z C(\mathbf{x}, z; \rho)$ the probability that isopycnal ρ sits at $(\mathbf{x}, z)$. These PDFs correspond, respectively, to the Eulerian and Lagrangian view. The mean density can be obtained as $\bar{\rho}(\mathbf{x}, z) = \int \rho P_E(\mathbf{x}, z; \rho)\, \mathrm{d}\rho$, so its RMS $\sigma_\rho^2(\mathbf{x}, z) = \int (\rho - \bar{\rho}(\mathbf{x}, z))^2 P_E(\mathbf{x}, z; \rho)\, \mathrm{d}\rho$. The isopycnal displacement $\zeta' = z - \bar{Z}(\mathbf{x}, \rho)$ requires a mean isopycnal depth $\bar{Z}(\mathbf{x}, \rho)$ that is computed with the Lagrangian PDF: $\bar{Z}(\mathbf{x}, \rho) = \int z P_L(\mathbf{x}, z; \rho)\, \mathrm{d}z$. The RMS of the isopycnal displacement is then $\sigma_\zeta^2(\mathbf{x}, \rho) = \int \zeta'^2 P_L(\mathbf{x}, \rho; z)\, \mathrm{d}z$. Note that in order for the vertical integral of P_L to be one, we set C to 1 at the surface (and 0 at the lowest depth, namely 2000 m). This amounts to fold the outcropped isopycnals at the surface (resp. 2000 m) and ensures robust estimations of $\bar{Z}$ and σ_ζ. Furthermore $\bar{\rho}(\mathbf{x}, z)$ and $Z(\mathbf{x}, \rho)$ represent a priori two different stratifications, although very close in the interior (Figure 1). They largely differ near the surface because the atmospheric forcing induces strong seasonal fluctuations of the density. This issue could be alleviated by using seasonal CDFs but at the expense of a reduced n. We use $\bar{Z}$ and its inverse mapping $\rho_{\text{ref}}(\mathbf{x}, z)$ as the reference profile for the EAPE computation. The EAPE density is then

$$\mathcal{V}(\mathbf{x}, z) = -\frac{g}{2\rho_0} \int \zeta'(\mathbf{x}, z; \rho) \rho'(\mathbf{x}, z; \rho)\, P_E(\mathbf{x}, z; \rho)\, \mathrm{d}\rho\,, \tag{3}$$

that is (1) but expressed with a PDF.

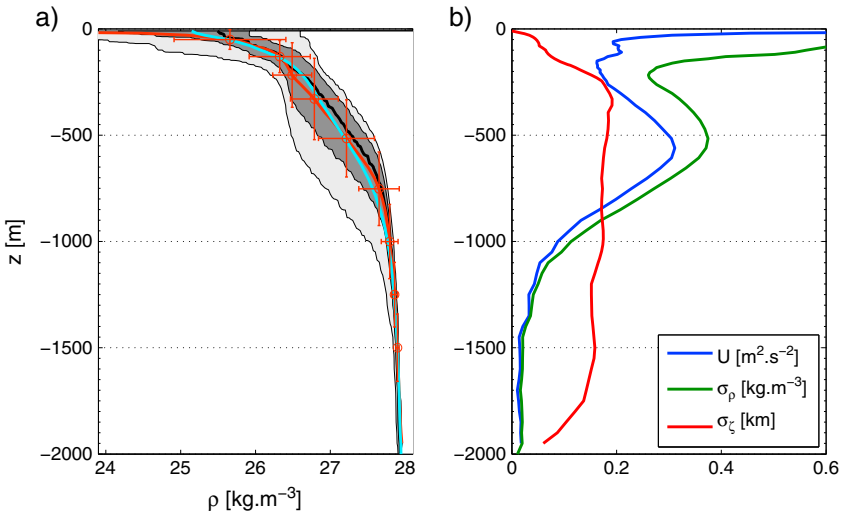

Figure 1. Statistical quantities at 60°W and 40°N. (a) Shaded areas correspond to the cumulative density function $C(z;\rho) \in [0.25\ 0.75]$ (dark gray) and [0.05 0.95] (light gray); thick lines are mean isopycnal depth $\bar{Z}(\rho)$ (red), mean density $\bar{\rho}(z)$ (cyan), median density (black), and bars represent RMS of density σ_ρ and RMS of vertical isopycnal displacement σ_ζ. (b) Vertical profiles of EAPE $\mathcal{U}$, σ_ρ, and σ_ζ.

3. The CDF and Its Associated Statistics

We illustrate the method (Figure 1) at 60°W–40°N, in the Gulf Stream region, a location archetypal of a high level of turbulence. The CDF (Figure 1a) has been estimated with $\sigma = 1/2°$, leading to $n(x,z) = 31$. The shaded areas in the (ρ, z) plane corresponds to where there is a 50% chance (dark gray) and a 90% (light gray) chance to measure ρ at depth z. The width of the area directly indicates the level of variability measured by σ_ρ and σ_ζ (bars in Figure 1a). The 0.5 isocontour of the CDF corresponds to the median density, close to $\bar{\rho}$. The two profiles ρ_{ref} and $\bar{\rho}$ (colored curves in Figure 1a) are very close except near the surface. In less energetic regions (not shown) the agreement is even better. Under the assumption of gaussian fluctuations, σ_ρ can be used to set a 95% confidence level on the mean climatology $\rho_{\text{clim}} = \bar{\rho} \pm 2\sigma_\rho/\sqrt{n}$. At this location, the uncertainty on the mean density climatology is thus smaller than the intrinsic variability by a factor of $\sqrt{n}/2 \approx 2.8$. As the Argo database fills up, this uncertainty will decrease.

Figure 1b shows the vertical profiles of the second order moments. As we generally find in most places, $\mathcal{U}$ and σ_ρ are surface intensified, whereas σ_ζ is larger at depth. The surface intensification (above 200 m) is mostly an artifact of annual means due to diabatic atmospheric forcings generating large density fluctuations. By redoing the same analysis (not shown) on seasons, we observe a much thinner CDF and large seasonal variations of $\bar{Z}$ close to the surface. These two effects cause the seasonal EAPE in the first 200 m to be smaller than annual EAPE by a factor ~2. In the interior, where isopycnals never reach the surface, we report that seasonal EAPE (not shown) also differs from annual EAPE, but the full description of the seasonal cycle deserves another study. A key feature of EAPE is the presence in some regions of an interior maximum (500 m at the chosen location of Figure 1b).

4. Maps of EAPE

We then present global maps of EAPE at three different depths (Figures 2a, 2c, and 2d) at the $\sigma = 1/2°$ resolution. The EKE map computed from AVISO sea level anomalies is also presented for comparison (Figure 2b). There is a striking agreement in the patterns and the magnitude of the two fields. This justifies the interest of looking at EAPE and should stimulate further studies on its coupling with the other forms of potential energy. It also argues that EAPE principally captures the mesoscale turbulence rather than the internal wave turbulence that has smaller isopycnal displacements [*Munk*, 1981]. The resemblance between EKE and EAPE can be explained in the quasi-geostrophic framework. EKE and EAPE are related to the vorticity and the stretching components of the potential vorticity which tend to be comparable at mesoscale.

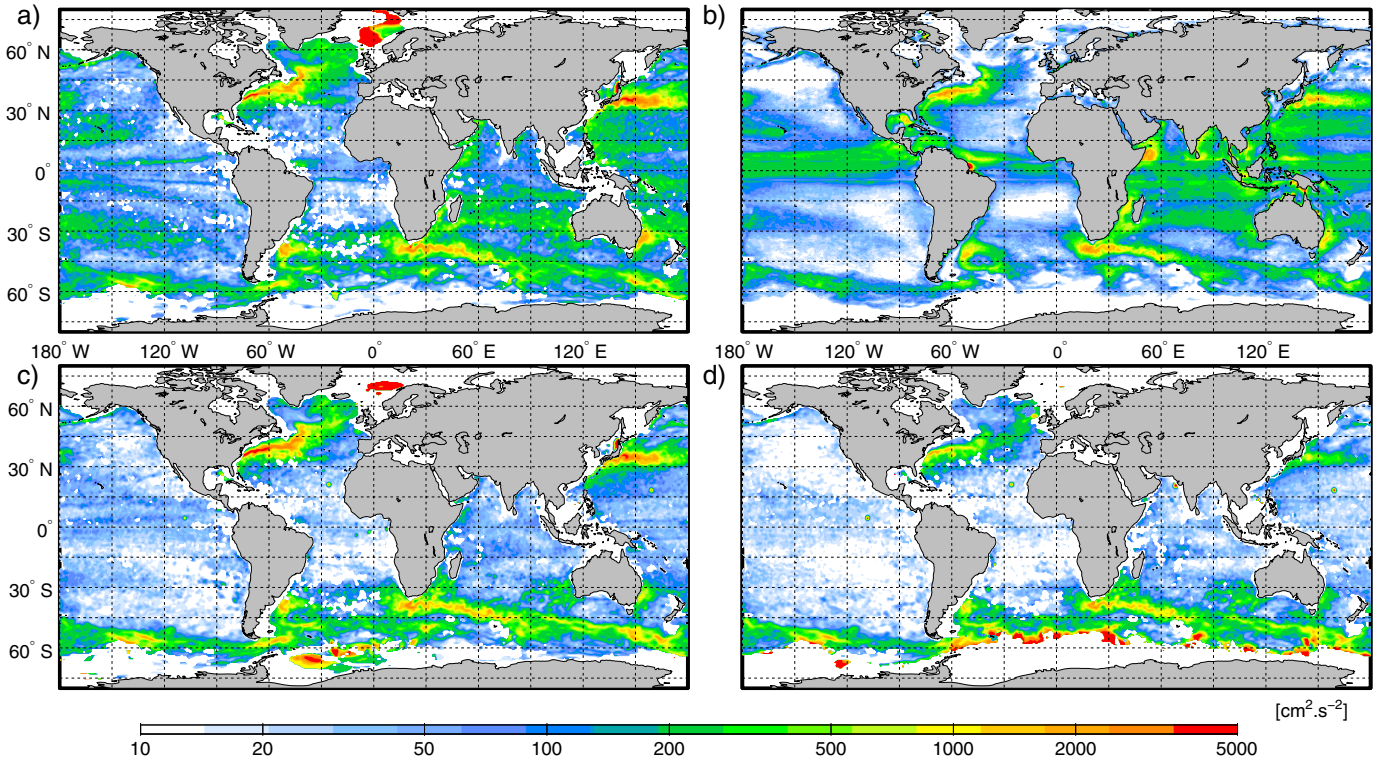

Figure 2. EAPE at (a) 250 m, (c) 500 m, and (d) 1000 m on a 1/2° × 1/2° grid, (b) EKE at surface as diagnosed from AVISO sea level anomalies measurements.

The three equatorial oceans have in common to be surface intensified with very little EAPE below 500 m for all longitudes. EAPE in the eastern Pacific Ocean exhibits patterns resembling Rossby rays [*Chelton and Schlax*, 1996] in the depth range 150–300 m (alternating bands of low and high EAPE, bending poleward toward the East); see for example the green streak connecting 180°W, 5°S and 90°W, 20°S in Figure 2a. It also reveals the turbulent intensity of equatorial quasi-zonal jets (Tsuchiya jets) located at about 6°S and 4°N [*Tsuchiya*, 1975]. These patterns are less pronounced in the Atlantic Ocean and absent in the Indian Ocean. The Indian Ocean is characterized by a relatively elevated EAPE between 30°S and 15°S compared to the two other oceans that is also visible in the EKE.

Overall, the main features are the western boundary currents and the Southern Ocean. They extend deeper than 1000 m. In the Southern Ocean EAPE and EKE have very similar patterns with extrema often colocated; see for instance 50°S–30°E, 50°S–150°E, and downstream Drake passage. The resolution is fine enough to reveal details of the mesoscale eddy field, e.g., associated with the Agulhas current retroflection, Agulhas return flow, and corridor of Agulhas rings. There is a clear evidence of standing meanders near 30°E. EAPE in the Gulf Stream region looks very similar to EKE, the branching of the Azores current is clear at 500 m depth. The peak value of EAPE at 500 m is roughly twice the peaks value of the surface EKE (4000 versus 2000 $cm^2\ s^{-2}$). An interesting difference between EAPE and EKE is in the North Atlantic Current, east of 30°W, where EAPE is larger by a factor of 10. This could be due to the weaker stratification that weakens the steric variations while it increases the vertical isopycnal displacements.

Lastly, we did not try to smooth the computed EAPE. Few outliers are visible. A large part of the noise comes from the yet too low number of profiles and from the disparity in the profiles density n (Figure 3a). The density reveals the already very good global coverage of the Argo database.

A typical EAPE vertical structure is shown along 120°W in Figure 4c. The chosen definition of EAPE is remarkably close to the quasi-geostrophic (QG) definition $\mathcal{V}_{QG} = g^2\overline{\rho'^2}/(2\rho_0^2 N_{BV}^2)$ (Figure 4d), where N_{BV} is the local climatological Brunt Vaisala frequency and for which $\zeta' = -gN_{BV}^2\rho'/\rho_0$, suggesting that the QG APE is a good approximation. However, a linear colorscale reveals that the latter yields smaller values for the interior maxima. The QG approximation relates the second moments with N_{BV}^2: $\mathcal{V} \sim N_{BV}^2\sigma_\zeta^2 \sim \sigma_\rho^2/N_{BV}^2$. EAPE has thus an intermediate vertical structure between σ_ζ and σ_ρ. We report, without explaining, that σ_ζ (Figure 4b) is

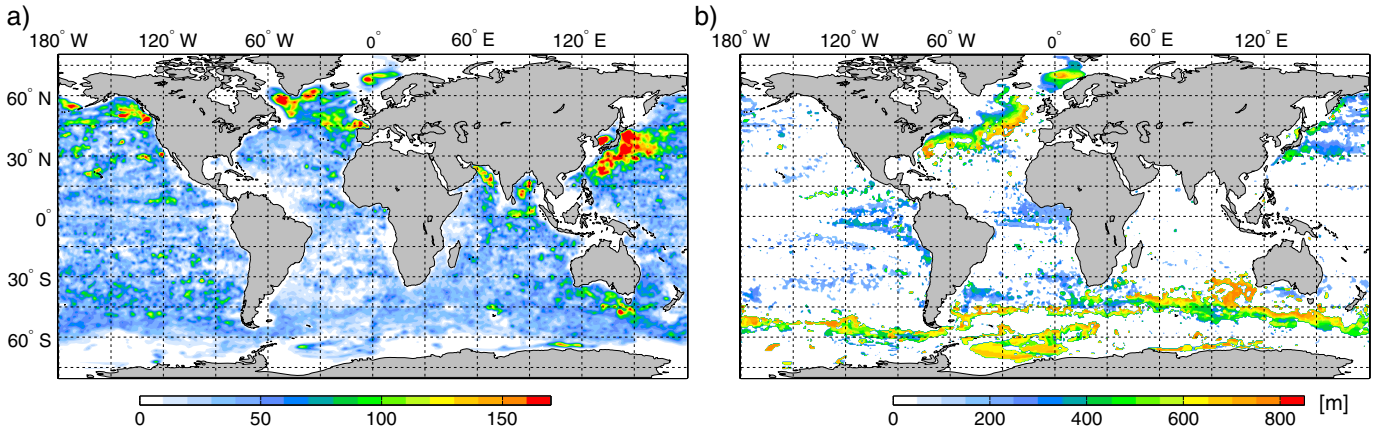

Figure 3. Number of profiles at 500 m (a), locations with less than 10 profiles are discarded. Depth of the interior maximum of EAPE (b) when it exists.

relatively uniform in the vertical and that it increases with latitude. Strongly surface intensified σ_ρ exhibits a rich spatial structure. The Antarctic Circumpolar Current (ACC) is clearly visible at 57°S and has an interior core of 800 cm^2 s^{-2} at ~700 m depth that coincides with a maximum of isopycnal slope. This feature is found everywhere in the Southern Ocean.

This interior maximum is likely an important dynamical feature because it suggests a local energy source. A good candidate for this source is the baroclinic instability which yields a conversion from mean potential to EKE and also to EAPE as defined herein. To confirm this interpretation we have systematically diagnosed the presence of an interior maximum on the EAPE profile (Figure 3b). To distinguish from the surface maximum, only maxima deeper than 200 m have been retained. Shallower maxima exist at some places, e.g., in eastern boundary upwellings. The places where the interior maximum exists and is deep (below 500 m) do also exhibit large EAPE. Deep maxima are conspicuously present all along the ACC at around 700 m and seem to be colocated with the depth of the maximum energy conversion [*Smith* [2007], Figure 8b], diagnosed indirectly with annual averages of temperature and salinity. This supports a connection between EAPE and active baroclinic instability.

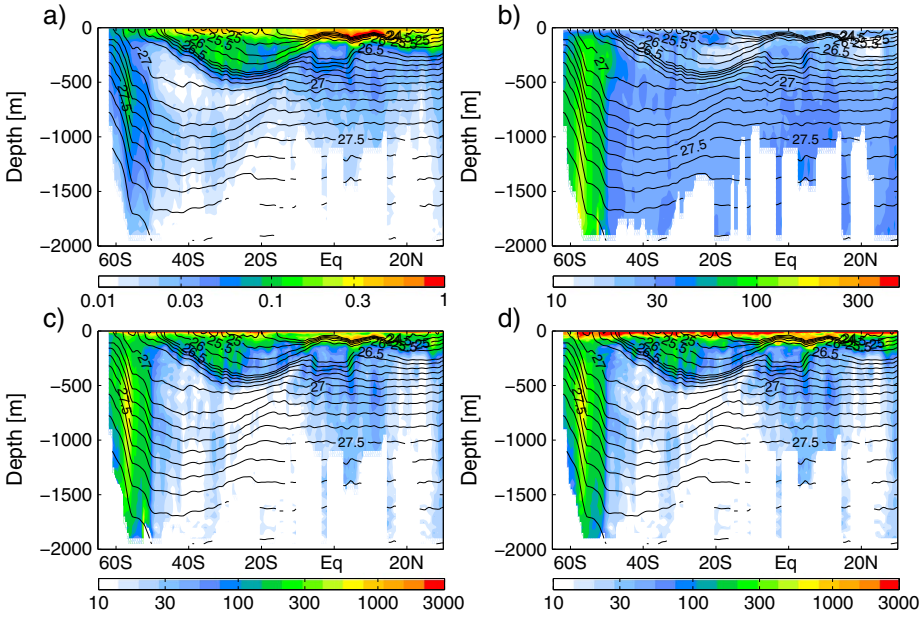

Figure 4. Vertical sections at 120°W of a) RMS of density σ_ρ (in kg m^{-3}), b) RMS of isopycnal displacement σ_ζ (in m), c) EAPE (in cm^2 s^{-2}) and d) quasi-geostrophic EAPE (in cm^2 s^{-2}). Superimposed are iso-contours of $\bar{\rho}^*$.

5. Conclusion

A new energy diagnostic of the mesoscale turbulence has been presented and used. It is defined as a second moment of the density PDF. It differs from a tracer variance [*Forget and Wunsch*, 2007; *Von Schuckmann et al.*, 2009] because it naturally connects to the ocean energy budget of ocean. By suitably gridding Argo data, we have estimated this PDF and produced maps of EAPE in the upper 2000 m of the World Ocean.

EAPE mainly reveals the internal structure of the mesoscale turbulence although it also contains the signature of internal wave activity. The patterns are very close to those of the surface EKE estimated from satellite altimetry while they are estimated via two completely independant data sets. EAPE is either monotically decreasing with depth or has an interior maximum. Wide zones of the ocean exhibit a deep secondary maximum of EAPE, below 200 m. We interpret these maxima as the signature of subsurface-intensified sources of mesoscale activity. These results open new routes to the use of Argo data, for example, in the evaluation of eddy-resolving ocean models.

Acknowledgments

This work was supported by French ANR SMOC. Argo data were collected and made freely available by the International Argo Program and the national programs that contribute to it. The altimeter products were produced by Ssalto/Duacs and distributed by Aviso, with support from Cnes.

The Editor thanks Gael Forget and an anonymous reviewer for their assistance in evaluating this paper.

References

Chelton, D. B., and M. G. Schlax (1996), Global observations of oceanic Rossby waves, *Science*, *272*, 234–238.

Chelton, D. B., M. G. Schlax, R. M. Samelson, and R. A. de Szoeke (2007), Global observations of large oceanic eddies, *Geophys. Res. Lett.*, *34*, L15606, doi:10.1029/2007GL030812.

Ducet, N., P. Y. Le Traon, and G. Reverdin (2000), Global high-resolution mapping of ocean circulation from TOPEX/Poseidon and ERS-1 and -2, *J. Geophys. Res.*, *105*(C8), 19,477–19,498.

Forget, G., and C. Wunsch (2007), Estimated global hydrographic variability, *J. Phys. Oceanogr.*, *37*(8), 1997–2008.

Hallberg, R. (2005), A thermobaric instability of Lagrangian vertical coordinate ocean models, *Ocean Modell.*, *8*(3), 279–300.

Holliday, D., and M. E. McIntyre (1980), On potential energy density in an incompressible stratified fluid, *J. Fluid Mech.*, *107*, 221–225.

Intergovernmental Oceanographic Commission, Scientific Committee on Oceanic Research, and International Association for Physical Sciences of the Oceans (2010), The international thermodynamic equation of seawater—2010: Calculation and use of thermodynamic properties, *Tech. Rep.*, Intergovernmental Oceanographic Commission.

Lorenz, E. (1955), Available potential energy and the maintenance of the general circulation, *Tellus*, *7*(2), 157–167.

Munk, W. (1981), Internal waves and small-scale processes, in *Evolution of Physical Oceanography*, edited by B. Warren and C. Wunsch, pp. 264–291, MIT Press, Cambridge, Mass.

Shchepetkin, A., and J. McWilliams (2011), Accurate Boussinesq oceanic modeling with a practical, Stiffened Equation of State, *Ocean Modell.*, *38*(1), 41–70.

Shepherd, T. G. (1993), A unified theory of available potential energy, *Atmos. Ocean*, *31*, 1–26.

Smith, K. (2007), The geography of linear baroclinic instability in Earth's oceans, *J. Mar. Res.*, *65*, 655–683.

Sun, S., R. Bleck, C. Rooth, J. Dukowicz, E. Chassignet, and P. Killworth (1999), Inclusion of thermobaricity in isopycnic-coordinate ocean models, *J. Phys. Oceanogr.*, *29*(10), 2719–2729.

Tailleux, R. (2012), Available potential energy and exergy in stratified fluids, *Annu. Rev. Fluid Mech.*, *45*(1), 35–58.

Tsuchiya, M. (1975), Subsurface countercurrents in the eastern equatorial Pacific Ocean, *J. Mar. Res.*, *33*, 145–175.

Von Schuckmann, K., F. Gaillard, and P.-Y. Le Traon (2009), Global hydrographic variability patterns during 2003–2008, *J. Geophys. Res.*, *114*, C09007, doi:10.1029/2008JC005237.

von Storch, J.-S., C. Eden, I. Fast, H. Haak, D. Hernández-Deckers, E. Maier-Reimer, J. Marotzke, and D. Stammer (2012), An estimate of the lorenz energy cycle for the world ocean based on the 1/10° storm/NCEP simulation, *J. Phys. Oceanogr.*, *42*(12), 2185–2205.